

# Geophysical Research Letters

## RESEARCH LETTER

10.1029/2019GL085758

### Key Points:

- We use a large ensemble of simulations to explore high-latitude climate seasonal shifts under stratospheric aerosol geoengineering
- Stratospheric aerosol geoengineering would alter seasonal cycle of temperature, snow depth, and sea ice at high latitudes
- Stratospheric heating and seasonal sunlight variations are two likely mechanisms that cause shifts in high-latitude seasonal cycle

### Supporting Information:

- Supporting Information S1

### Correspondence to:

L. Cao,  
longcao@zju.edu.cn

### Citation:

Jiang, J., Cao, L., MacMartin, D. G., Simpson, I. R., Kravitz, B., Cheng, W., et al. (2019). Stratospheric sulfate aerosol geoengineering could alter the high-latitude seasonal cycle.

*Geophysical Research Letters*, 46, 14,153–14,163. <https://doi.org/10.1029/2019GL085758>

Received 14 OCT 2019

Accepted 23 NOV 2019

Accepted article online 3 DEC 2019

Published online 6 DEC 2019

## Stratospheric Sulfate Aerosol Geoengineering Could Alter the High-Latitude Seasonal Cycle

Jiu Jiang<sup>1</sup>, Long Cao<sup>1</sup>, Douglas G. MacMartin<sup>2</sup>, Isla R. Simpson<sup>3</sup>, Ben Kravitz<sup>4,5</sup>, Wei Cheng<sup>2</sup>, Daniele Visioni<sup>2</sup>, Simone Tilmes<sup>6</sup>, Jadwiga H. Richter<sup>3</sup>, and Michael J. Mills<sup>6</sup>

<sup>1</sup>Department of Atmospheric Sciences, School of Earth Sciences, Zhejiang University, Hangzhou, China, <sup>2</sup>Mechanical and Aerospace Engineering, Cornell University, Ithaca, NY, USA, <sup>3</sup>Climate and Global Dynamics Laboratory, National Center for Atmospheric Research, Boulder, CO, USA, <sup>4</sup>Department of Earth and Atmospheric Sciences, Indiana University, Bloomington, IN, USA, <sup>5</sup>Atmospheric Sciences and Global Change Division, Pacific Northwest National Laboratory, Richland, WA, USA, <sup>6</sup>Atmospheric Chemistry, Observations, and Modeling Laboratory, National Center for Atmospheric Research, Boulder, CO, USA

**Abstract** Stratospheric aerosol geoengineering (SAG) has been proposed to reduce some impacts of anthropogenic climate change. Previous studies examined annual mean climate responses to SAG. Here we use the Stratospheric Aerosol Geoengineering Large Ensemble simulations to explore the effects of SAG on the seasonal cycle of climate change. Simulations show that relative to the present-day climate, SAG diminishes the amplitude of the seasonal cycle of temperature at many high-latitude locations, with warmer winters and cooler summers. The seasonal temperature shift significantly influences the seasonal cycle of snow depth and sea ice, with Arctic sea ice recovery overcompensated in summer by 52% and undercompensated in winter by 8%. We identify that both the dynamic effects of aerosol-induced stratospheric heating and seasonal variations of sunlight contribute to the shifts in seasonal cycle. Shifts in the seasonal cycle have important ecological and environmental implications, which should be considered in geoengineering impact analysis.

**Plain Language Summary** Stratospheric aerosol geoengineering, by releasing sulfate aerosol particles or their precursors ( $\text{SO}_2$ ) into the stratosphere to scatter more sunlight back to space, is a potential climate intervention option to counteract anthropogenic global warming. Previous studies focused on the effect of aerosol injection on annual mean climate change. Here we assess seasonal climate shifts in response to aerosol injection using a large ensemble of sophisticated climate model simulations. Relative to the high- $\text{CO}_2$  scenario, stratospheric aerosol injection can stabilize many aspects of climate change on the annual mean basis including global mean temperature, interhemispheric temperature gradient, and equator-to-pole temperature gradient. However, we find that injection of  $\text{SO}_2$  into the stratosphere would substantially alter the high-latitude seasonal cycle. Relative to the present-day climate, in a high- $\text{CO}_2$  world with additional aerosols in the stratosphere, many high-latitude locations are warmer in winter and cooler in summer. Meanwhile, stratospheric aerosol geoengineering overcompensated Arctic sea ice extent recovery in summer and undercompensated it in winter. These seasonal climate shifts have important ecological, economic, and aesthetic implications for a full assessment of benefits and risks of stratospheric aerosol geoengineering.

### 1. Introduction

Mitigation of anthropogenic  $\text{CO}_2$  emissions may be insufficient to avoid significant risks from climate change (Rogelj et al., 2016). Solar geoengineering could be a potential means to rapidly alleviate some of the detrimental consequences of global warming induced by increasing atmospheric  $\text{CO}_2$  concentrations (Irvine et al., 2016; Keith, 2000; National Research Council, 2015).

Stratospheric aerosol geoengineering (SAG) using sulfate aerosol particles or their precursors is a proposed solar geoengineering scheme that has been widely studied (e.g., Crutzen, 2006; Rasch et al., 2008; Rasch et al., 2008; Robock et al., 2008; National Research Council, 2015; Niemeier & Timmreck, 2015; Ferraro & Griffiths, 2016). A sustained layer of additional sulfate aerosols in the stratosphere would scatter some of the incoming solar radiation back to space, cooling the Earth. Numerous climate modeling studies on SAG have suggested that it could reduce many impacts of anthropogenic global warming, such as sea

level rise, floods, permafrost degradation, and extreme weather (e.g., Rasch et al., 2008; Moore et al., 2010; Irvine et al., 2016; Wei et al., 2018; Ji et al., 2018; Lee et al., 2019), and also have side effects such as decreased stratospheric ozone concentrations in polar regions (Pitari et al., 2014; Tilmes et al., 2008).

Most studies of the impacts of SAG have focused on annual mean change in climate variables (Irvine et al., 2016; National Research Council, 2015). It is expected that SAG would also affect the seasonal cycle. Two primary mechanisms would likely contribute to the shift in the seasonal cycle in the geoengineered world with high atmospheric CO<sub>2</sub>. First, compared to the radiative forcing of atmospheric CO<sub>2</sub>, solar forcing has a much larger seasonal variation (Govindasamy et al., 2000, 2003). There is more sunlight to reflect in the summer, especially at high latitudes, and thus, solar geoengineering would diminish the seasonal amplitude of surface temperature, in particular in the high-latitude regions (Govindasamy et al., 2000, 2003). Second, sulfate aerosols absorb infrared radiation and heat the stratosphere (Stenchikov et al., 1998). The stratospheric heating could have significant dynamic effects on many aspects of the climate system (Ferraro et al., 2014; Ferraro et al., 2015; Richter et al., 2017; Visioni et al., 2017), including Northern Hemisphere (NH) winter warming that has been observed after large volcanic eruptions (Driscoll et al., 2012; Robock & Mao, 1992; Shindell et al., 2004; Wunderlich & Mitchell, 2017). Although volcanic eruptions are an imperfect analog of SAG, SAG-induced stratospheric dynamic change could also lead to the NH winter warming (Rasch et al., 2008; Kravitz et al., 2019).

In this study, we investigate the seasonal climate response to SAG using the 20-member Stratospheric Aerosol Geoengineering Large Ensemble (GLENS, described in detail by Tilmes et al., 2018). This is the first large ensemble project for evaluating the impact of solar geoengineering, providing a better estimate of the forced response to the chosen scenario in the presence of natural variability. GLENS utilizes a feedback control algorithm to annually adjust SO<sub>2</sub> injection rates at four independent locations to stabilize three temperature features simultaneously at their 2020 levels: annual and global mean surface air temperature, annual mean interhemispheric temperature gradient, and annual mean equator-to-pole temperature gradients. This strategic geoengineering approach is implemented in the Community Earth System Model (CESM) version 1 with the Whole Atmosphere Community Climate Model (WACCM) as its atmospheric component (see section 2), under a *no policy* climate scenario (Representative Concentration Pathway 8.5, RCP8.5, van Vuuren et al., 2011) during the 21st century (Tilmes et al., 2018).

We observe that the seasonal cycle of temperature over high-latitude areas is altered in GLENS simulations. This leads to significant changes of seasonality in the high-latitude cryosphere, especially for the Arctic sea ice and snow depth. To better understand the mechanisms of high-latitude seasonal cycle shifts, in section 4 we compare our results with those from stratospheric heating experiments (Simpson et al., 2019) as well as solar dimming simulations (Kravitz et al., 2016).

## 2. Methods

### 2.1. GLENS Model and Experiment Description

All simulations from the GLENS are performed with the CESM version 1 (CESM1; Hurrell et al., 2013), incorporating the WACCM as the atmospheric component (CESM1[WACCM]), and fully coupled to land, ocean, and sea ice models (Mills et al., 2017). The atmospheric component has 72 vertical layers up to 140-km altitude, with a horizontal resolution of 0.9° latitude by 1.25° longitude. There is a comprehensive treatment in the model of stratospheric sulfate aerosol formation, microphysical growth processes, and sedimentation, using a modal representation of aerosols (the three-mode version of the Modal Aerosol Module, Liu et al., 2012). Also, the model includes a fully interactive stratospheric chemistry and atmospheric dynamics including an internally generated quasi-biennial oscillation. These processes influence the stratospheric circulation and consequently the spatial distribution of sulfate aerosols (Richter et al., 2017). The detailed validation and features of CESM1(WACCM) are described by Mills et al. (2017), except that (as noted by Tilmes et al., 2018) the land component used here is the Community Land Model version 4.5 (CLM4.5) as described by Oleson et al. (2013). Mills et al. (2017) has validated that this model configuration reasonably reproduce present-day quasi-biennial oscillation, stratospheric ozone, and water vapor concentration. Also, the model-simulated changes in radiative forcing following the 1991 Pinatubo eruption compare reasonably well with observation-based estimates (Mills et al., 2017), providing confidence for the model-simulated climate response to stratospheric aerosol geoengineering.

The detailed description of GLENS simulations is provided by Tilmes et al. (2018). The GLENS simulations are conducted under specified greenhouse gas concentrations following the representative concentration pathway 8.5 (RCP8.5, Meinshausen et al., 2011; van Vuuren et al., 2011). For the RCP8.5 simulations, a 20-member ensemble is performed over the time period of 2010–2030, with three ensemble members extended until at least 2097. The stratospheric sulfate aerosol geoengineering simulations are branched from each of the 20 RCP8.5 simulations in 2020 and extended until 2099. In the geoengineering simulations, SO<sub>2</sub> is injected into the stratosphere at four different injection locations (15°N and 15°S at 25 km, 30°N and 30°S at 22.8 km, all at 180° longitude). GLENS employs a feedback algorithm to annually adjust SO<sub>2</sub> injection rates independently at each location with the goal to simultaneously maintain the global mean temperature and the interhemispheric and equator-to-pole temperature gradients at 2020 levels (see Kravitz et al., 2017 for a detailed description of the setup and objectives). In this study, we use the model output averaged between 2010 and 2030 from the RCP8.5 simulations as the baseline (Tilmes et al., 2018). For the evaluation of changes under geoengineering, we use the average over 2075–2095, relative to the baseline. This time period, in which geoengineering is providing 5.0 K cooling, is used to provide a high signal-to-noise ratio in understanding the effects.

Numerous studies have evaluated the performance of the CESM in simulating high-latitude climate. Kay et al. (2014) performed a 30-member CESM large ensemble (CESM-LE) using CESM1 version 1 with the Community Atmosphere Model version 5 (CAM5). These simulation results show that the CESM-simulated historical trend of Arctic sea ice, as well as the sea ice thickness, compares reasonably with observations (Barnhart et al., 2015; Jahn et al., 2016; Labe et al., 2018). Also, CESM-simulated sea ice motion over the Arctic Ocean compares reasonably with available observations (DeRepentigny et al., 2016).

## 2.2. Diagnostic Method of Permafrost

Near-surface permafrost is diagnosed in the model simulations by detecting whether the ground soil temperature is at or below 0 °C for 24 consecutive months (Slater & Lawrence, 2013). In practice, in our diagnostic of permafrost, for a model grid cell, if any of the soil layer above 3.5 m has a temperature at or below 0 °C for 24 consecutive months, the model grid is considered to be permafrost. Previous modeling simulations with the land component CLM4 showed that the model-simulated permafrost distribution reasonably matches the observed distribution and broadly captures the southern edge of permafrost across the circum-Arctic permafrost regions (Lawrence et al., 2012).

The land component used for GLENS is CLM4.5. Compared to CLM4.0, it includes an active terrestrial carbon cycle with photosynthesis and respiration and considers different pools of nitrogen and carbon (Oleson et al., 2017). As an updated version, CLM4.5 is supposed to share the ability of CLM4.0 in simulating permafrost. Present-day near-surface permafrost extent simulated by CLM4.5 is 18.6 million km<sup>2</sup>, which is comparable to the observation-based estimation of 16.2 million km<sup>2</sup> (Brown et al., 2002).

## 2.3. Description of GEOHEAT, GEOHEAT\_S, and 3 × 3 Simulations

In this study, we compare our results with two related geoengineering simulations also conducted using CESM1. Simpson et al. (2019) performed a four-member ensemble of simulations, referred to as GEOHEAT, under RCP8.5 radiative forcing from 2010 to 2030 with additional stratospheric heating imposed. This heating was derived from GLENS over the time period from 2075 to 2095 and represents the radiative heating rates due to the excess sulfate aerosol as determined by a double call to the radiation scheme: in one call the radiation scheme saw the aerosols and in the other it did not. In GEOHEAT, some global mean warming of about 0.6 K arises as a result of the greenhouse effect of increased stratospheric water vapor. To minimize the warming, Simpson et al. (2019) also conducted a short-term spin-up ensemble (GEOHEAT\_S). GEOHEAT\_S has the same additional stratospheric heating imposed as in GEOHEAT, but each member of GEOHEAT\_S is initialized from 1 January of each year of the baseline simulations and run for 14 months to avoid the substantial change of stratospheric water vapor. The annual mean climate variables for GEOHEAT\_S are taken from March of the first year to February of the second year.

Kravitz et al. (2016) conducted a 70-year simulation of a designed solar-reduction strategy referred to as the 3 × 3 case, indicating the number of modified degrees of freedom and the number of climate targets. They performed simulations under prescribed CO<sub>2</sub> concentrations with a 1% increase per year, using a version of CESM that has a different atmospheric component (CAM5) and land model version (CLM4) compared to

that of GLENS. Also, the RCP8.5 scenario used in GLENS involves changes in tropospheric aerosols and land use, which are not present in the idealized  $3 \times 3$  case with 1% CO<sub>2</sub>/year increase. In the  $3 \times 3$  case, insolation is reduced to minimize the changes in the global mean temperature, and the interhemispheric and equator-to-pole temperature gradients: these are the same climate objective as in GLENS. To compare the GLENS and  $3 \times 3$  case, we choose the time period of GLENS and the  $3 \times 3$  case that has the same amount of cooling relative to their own high-CO<sub>2</sub> background. For the  $3 \times 3$  case, we choose the time period between years 40–70, during which the cooling caused by solar reduction (relative to the 1% CO<sub>2</sub> increase) is 2.3 K. For GLENS, we choose the time period between years 2040 and 2060, during which the cooling caused by aerosol injection (relative to RCP8.5) is also 2.3 K.

### 3. Shifts in the High-Latitude Climate Seasonal Cycle

In this section, we discuss shifts in the seasonal cycle simulated by GLENS focusing on the high-latitude cryosphere. All reported changes are for the period 2075–2095 relative to the baseline (ensemble mean of RCP8.5 simulations during 2010–2030).

By design, in terms of annual mean values, GLENS simulations successfully maintain the global mean surface air temperature at the baseline level and minimize changes in both the interhemispheric and equator-to-pole temperature gradients (Tilmes et al., 2018). Nonetheless, temperatures depart from the baseline at the regional scale (Figure 1a).

Relative to the baseline, the surface air temperature change over the high latitudes under GLENS exhibits substantial shifts in the seasonal cycle (see Figure 1 for residual changes and Figure S1 in the supporting information for absolute changes). To isolate seasonal shifts from residual warming that is present all year, we show the departures of the boreal summer June-July-August (JJA) and winter December-January-February (DJF) temperature changes relative to the annual mean temperature changes (Figures 1b and 1c). Over high-latitude land in both hemispheres, relative to baseline, JJA and DJF temperatures have opposite signs of change with warming in winter and cooling in summer, illustrating a diminished seasonal cycle under GLENS (Figures 1b and 1c). We also note that under GLENS, in the near-polar Arctic Ocean (around 85°N–90°N), both JJA and DJF are relatively warmer than the annual mean change. The reason is that sea ice increases sufficiently in September-October-November (SON) to generate a considerable cooling in SON, and all other seasons are relatively warmer than the average (Figure S2). The seasonal cycle of temperature in the northern high latitudes is roughly sinusoidal (Figure S3a). The maximum reduction in temperature seasonal cycle amplitude appears in northern Scandinavia ( $40.3 \pm 0.8\%$ ), but there are also places where the seasonal cycle amplitude increases, with a maximum increase of  $19.5 \pm 0.5\%$  in Nunavut (Figure S3b).

The residual winter warming could have substantial effects on the high-latitude cryosphere at some specific locations. For example, in places such as Helsinki and Stockholm where the winter is slightly below or around freezing, a slightly warmer winter in response to SAG as simulated in GLENS would cause a considerable decrease in the snow depth relative to the baseline, though snow depth is still greater than under RCP8.5 (Figure 2). Changes in snowfall, both in timing and in amount, were frequently brought up in a focus-group study in northern Finland as an important concern for climate change, with economic, ecological, and aesthetic dimensions (Buck, 2018).

Under RCP8.5, sea ice extents in high latitudes experience rapid decrease during this century, while GLENS largely maintains the high-latitude sea ice in both hemispheres (Figure S4, also see Kravitz et al., 2019). However, the seasonal temperature shift at high latitudes under GLENS has a significant effect on the seasonal cycle of sea ice change. As shown in Figure 3, under GLENS, the Arctic sea ice extent decreases over baseline levels during boreal winter and increases during summer, with an 8% reduction in March (when sea ice extent reaches maximum in the baseline) and a 52% increase in September (when sea ice extent reaches minimum in the baseline) (Figure 3a). Antarctic sea ice extent in GLENS exhibits a 23% reduction during austral winter, while only a slight shift in sea ice occurs during summer (Figure 3b). Figure S5 show the Arctic sea ice extent loss in March and gain in September under GLENS relative to the baseline. In the NH, decreases in the March Arctic sea ice concentration in GLENS are most pronounced in regions around Greenland and Alaska, and the Barents-Kara Seas (Figure 3c), and increases in the September Arctic sea ice concentration span much of the Arctic Ocean (Figure 3e), which correlates well with the distribution of

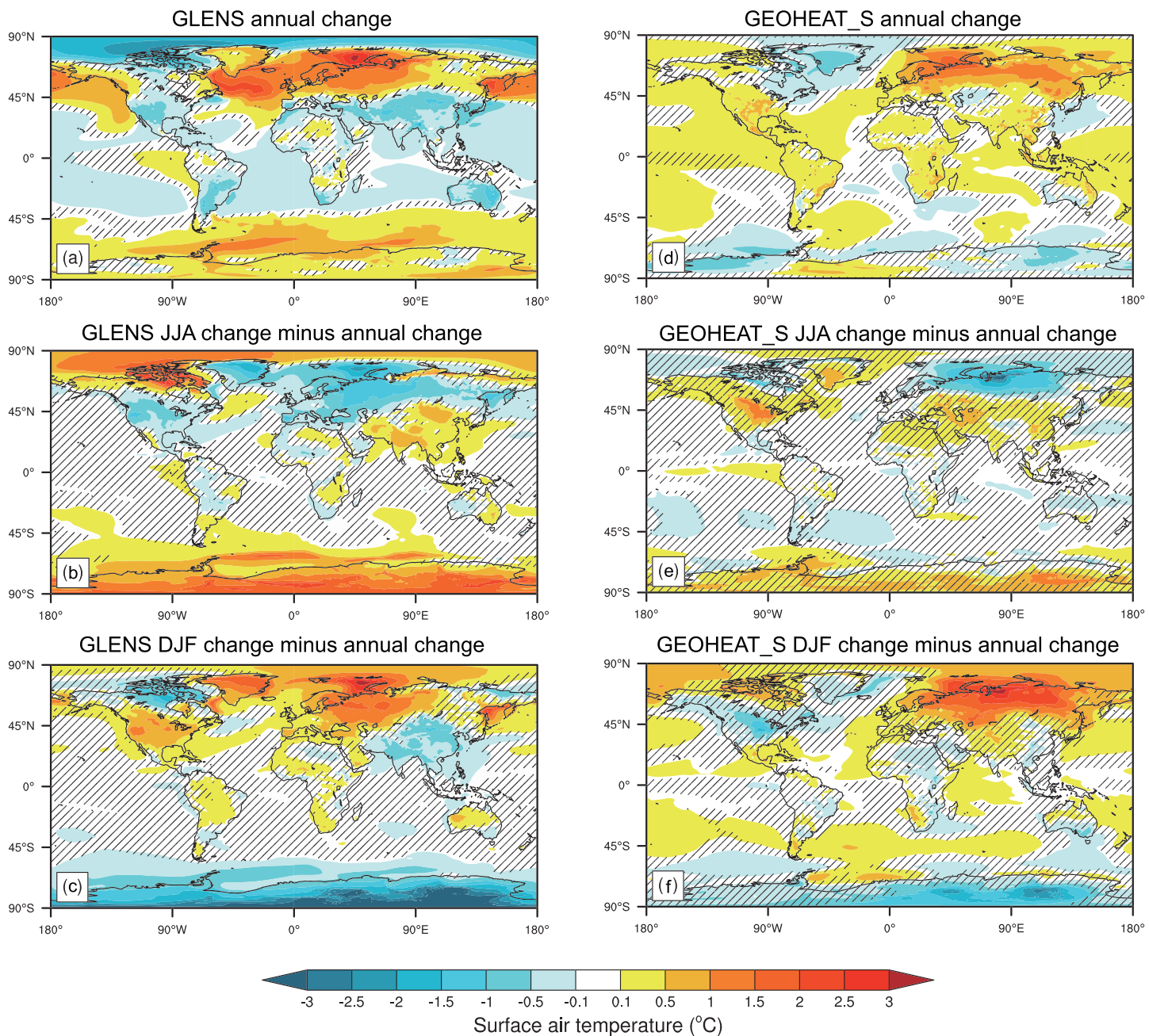


**Figure 1.** Annual and seasonal surface temperature change for GLENS (left column) and GEOHEAT\_S (right column) simulations. Annual mean change (a), JJA change minus annual mean change (b), and DJF change minus annual mean change (c) of temperature for GLENS. Annual mean change (d), JJA change minus annual mean change (e), and DJF change minus annual mean change (f) of temperature for GEOHEAT\_S. For GLENS, changes represent departures of the 2075–2095 ensemble mean from the baseline RCP8.5 2010–2030 ensemble mean. For GEOHEAT\_S, changes represent departures of GEOHEAT\_S (2010–2030) from the baseline (RCP8.5 2010–2030) mean. Hatched areas are regions where the changes are not statistically significant at the 5% level by the Student's *t* test.

temperature change (Figure S5). On the other hand, changes in atmospheric circulation, ocean currents and mixing, and ocean heat flux could also affect the sea ice response at local scale (Moore et al., 2014). In the Southern Hemisphere (SH), compared to the baseline, the Antarctic sea ice concentration under GLENS decreases across much of the ocean around Antarctic in September (Figure 3f). During the austral summer, sea surface temperature around Antarctica is warmer in GLENS compared to the baseline (Figure S6), which leads to a slight decrease in total Antarctic sea ice extent in austral summer relative to the baseline (Figure 3b). The result reported by Moore et al. (2014) shows that there is only a slight

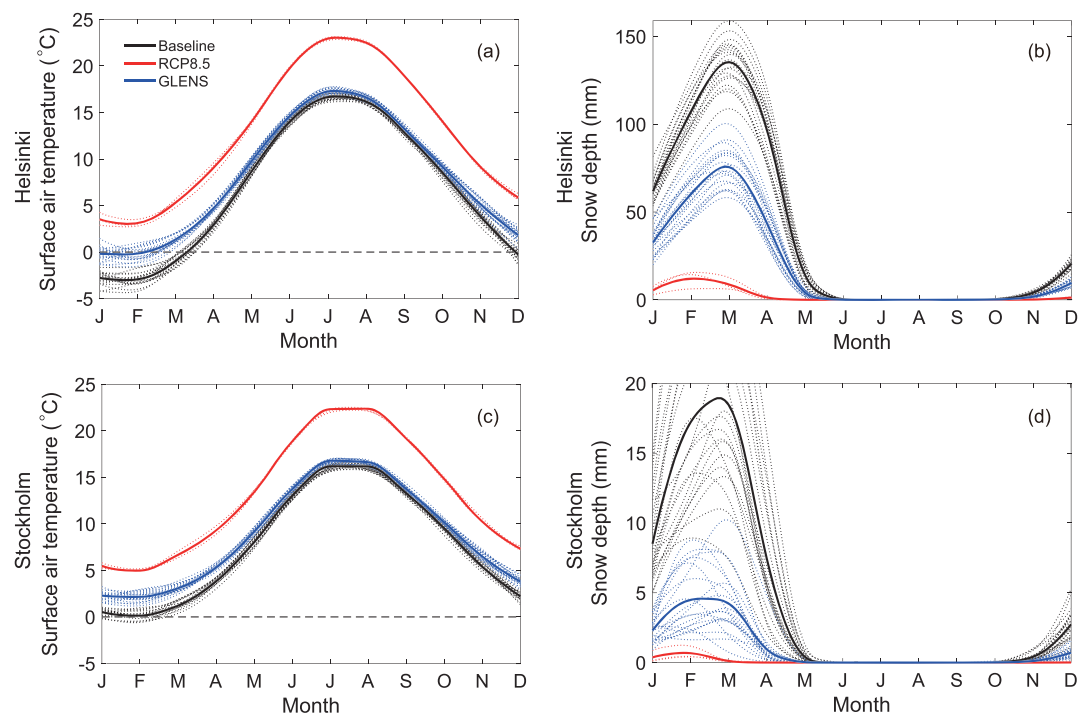


**Figure 2.** Model-simulated monthly-mean surface air temperature (a) and snow depth (b) at Helsinki ( $60.2^{\circ}\text{N}$ ,  $24.9^{\circ}\text{E}$ ), and surface air temperature (c) and snow depth (d) at Stockholm ( $59.3^{\circ}\text{N}$ ,  $18.0^{\circ}\text{E}$ ). The ensemble mean results are shown with the solid lines, and single ensemble members are shown with the dotted lines. The black lines are for baseline (RCP8.5 2010–2030) results; the red lines are for RCP8.5 2075–2095 results; the blue lines are for GLENS 2075–2095 results.

seasonal cycle change in the Arctic sea ice extent under G1 (the G1 scenario uses insolation reduction to balance the radiative forcing from an abrupt quadrupling  $\text{CO}_2$ ), which is different from our result here, indicating that solar reduction does not sufficiently capture some relevant seasonal effects from stratospheric aerosol injections.

Not all fields related to the cryosphere are strongly influenced by the shift in the seasonal cycle of temperature under GLENS. Near-surface permafrost is diagnosed in the model simulations by accounting for the areas where the ground soil (soil depth above 3.5 m, see section 2) is frozen for at least two consecutive years (Slater & Lawrence, 2013). Relative to the baseline, under RCP8.5, Arctic annual mean permafrost area decreases by 83% by the end of this century, whereas the decrease is only 5% in GLENS (Figure S7a). The spatial pattern of the Arctic permafrost area under GLENS is similar to the baseline with slight changes at the margin areas (Figure S7b). Compared to the baseline, the shift in the seasonal cycle of permafrost is not statistically significant (Figure S8a), which is consistent with the nonsignificant shift in the seasonal cycle of soil temperature in the top 3.5 m (Figures S8b and S8c). The seasonal cycle of temperature is much weaker below the surface, and thus, changes in the seasonal cycle of surface temperature are less important in influencing permafrost area than the residual changes in the annual mean temperature.

For land ice sheets, Greenland runoff accounts for about half of present-day ice loss and is thus a relevant metric for ice sheet mass balance (van den Broeke et al., 2009). In both RCP8.5 and GLENS simulations, the difference between precipitation and evapotranspiration (P-E) contributes to about half of the increase in Greenland runoff (Figure S9), indicating that about half of the increase in Greenland runoff stems from glacier melting. Relative to RCP8.5, the annual mean Greenland runoff under GLENS is largely maintained at 2020 level during the time period of 2020–2100 (Figure S7c). In GLENS there is a small but statistically significant reduction in seasonal cycle amplitude of Greenland runoff (Figure S7d), which is consistent with the seasonal cycle changes in high-latitude temperature. It should be noted that the model does not include dynamic ice sheets and that the measure of runoff is purely diagnostic based on the surface energy balance and does not actually affect the ice sheet in the model.

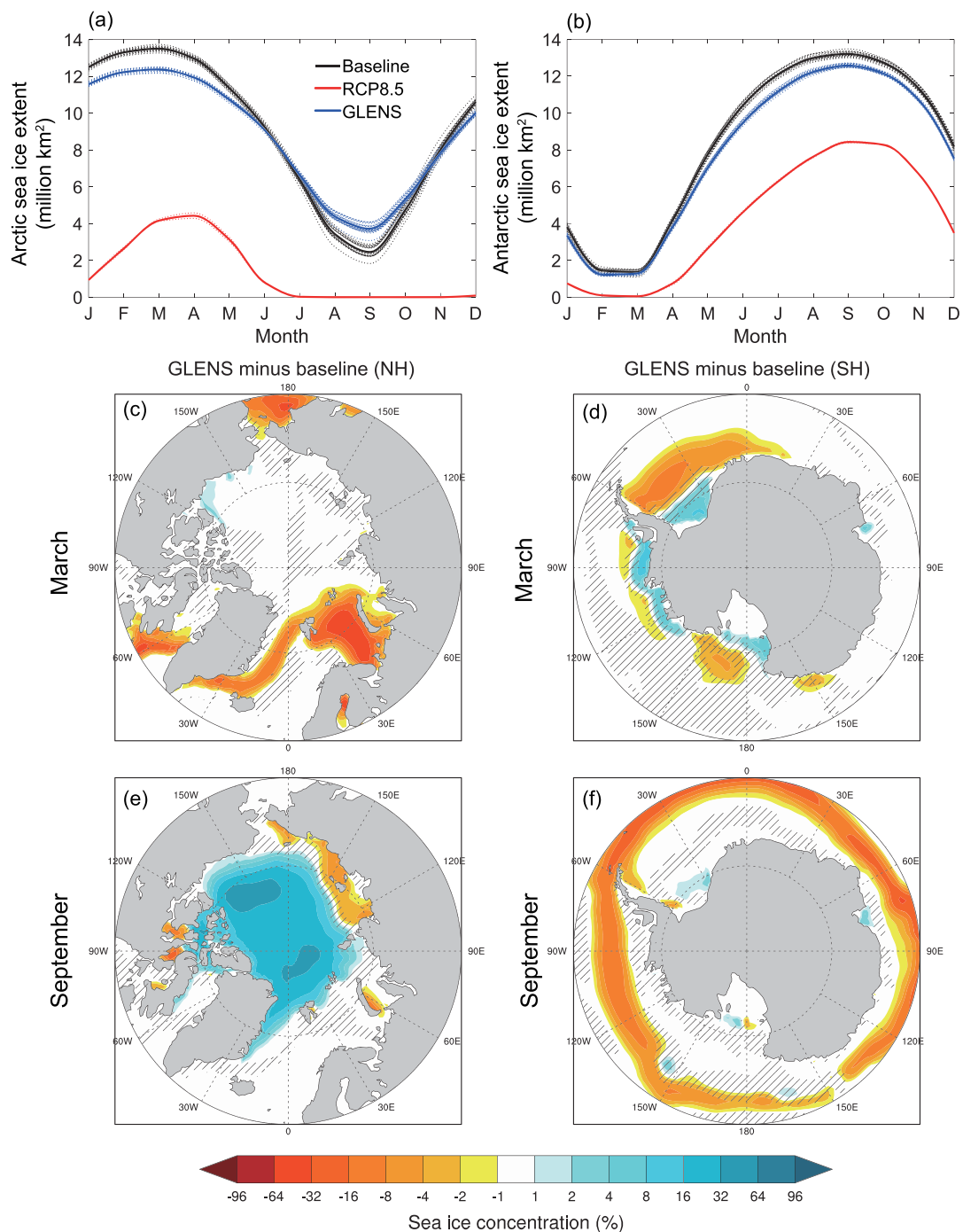


**Figure 3.** Model-simulated monthly-mean sea ice extent of (a) Arctic (north of 60°N) and (b) Antarctic (south of 60°S) for baseline (RCP8.5 2010–2030, black lines), RCP8.5 (2075–2095, red lines), and GLENS (2075–2095, blue lines). The ensemble mean results are shown with the solid lines, and the single ensemble members are shown with the dotted lines. Model-simulated ensemble mean sea ice concentration change (%) under GLENS (2075–2095) relative to baseline (RCP8.5 2010–2030) in March over (c) Arctic (north of 60°N) and (d) Antarctic (south of 60°S) and in September over (e) Arctic and (f) Antarctic. Hatched areas are regions where the changes are not statistically significant at the 5% level by the Student's *t* test.

#### 4. Mechanisms

Two likely mechanisms could lead to shifts in the seasonal cycle of temperature and other variables at high latitudes in GLENS: the seasonal variation of sunlight and the dynamic effect of stratospheric heating. The effect of seasonal variation of sunlight is partially compensated by the seasonal dependence of aerosol optical depth (AOD) with higher AOD in winter and lower AOD in summer over high latitudes (Figure S10). To better understand the contribution of these two mechanisms to changes in the high-latitude seasonal cycle, we compare the temperature seasonal cycle in GLENS with the results of two relevant simulations.

Simpson et al. (2019) conducted a set of simulations with the same CESM model version as GLENS, referred to as GEOHEAT, in which the additional stratospheric heating caused by the injected sulfate aerosols in GLENS in 2075–2095 was added over the baseline 2010–2030 period but without the aerosol injection. In this way, the impacts of stratospheric heating can be isolated from the scattering effect of stratospheric aerosols and the radiative impact of higher greenhouse gas concentrations. In GEOHEAT, a surface warming of about 0.6 K is observed, which likely arises from enhanced stratospheric water vapor concentration. To reduce the effect of the warming, Simpson et al also considered a short-term spin-up ensemble (GEOHEAT\_S) to avoid changes in stratospheric water vapor and hence reduce the global warming relative to GEOHEAT (GEOHEAT and GEOHEAT\_S are described in detail in section 2). Figure 1 shows the seasonal temperature anomalies for GLENS (left column) and GEOHEAT\_S (right column), both of which have near-zero global mean surface warming. Temperature seasonal changes in GEOHEAT are shown in Figure S11.

In the NH, GLENS, GEOHEAT, and GEOHEAT\_S have similar spatial patterns and magnitudes of temperature seasonal cycle change over most regions in Scandinavia and Russia (Figure 1), indicating that the dynamic effect of stratospheric heating contributes at least partly to the NH high-latitude seasonal cycle shifts in GLENS. A similar warm anomaly in boreal winter over northern Europe is also seen after volcanic eruptions (Driscoll et al., 2012; Wunderlich & Mitchell, 2017). Following large volcanic eruptions, aerosol-induced stratospheric heating and the associated strengthening of the stratospheric polar vortex would generate a poleward shift of the Atlantic jet, which is associated with increased zonal advection of warm maritime air over the continent, giving rise to the warming in northern Europe. This pattern of temperature change is quite analogous to what happens in association with the North Atlantic Oscillation variability, which is often influenced by stratospheric vortex variability (Thompson & Wallace, 2001). However, from Figure 1, the seasonal cycle shift is quite different between GLENS and GEOHEAT\_S over Greenland and north of Canada. This could be a result of the fact that there is no sustained ocean response in GEOHEAT\_S. Such differences also occur when comparing GLENS and GEOHEAT (Figure S11). Under GLENS, the Atlantic meridional overturning circulation strengthens considerably after year 2030 to the end of this century, which increases ocean heat transport and consequently warming at high latitudes (Fasullo et al., 2018), while the Atlantic meridional overturning circulation might not have fully responded in GEOHEAT.

In the SH high latitudes, GLENS and GEOHEAT\_S show a similar spatial distribution of temperature seasonal shifts over Antarctica (Figure 1). However, GEOHEAT has the opposite effect on the temperature seasonal cycle in Antarctica (i.e., relatively cooler winters and relatively warmer summers) compared to GLENS and GEOHEAT\_S (Figures 1 and S11). Stratospheric heating would result in a poleward shift of both the Atlantic jet and the SH jet. A poleward shift of the Atlantic jet would be expected to result in warming over northern Europe due to increased zonal advection of warm air from the Atlantic ocean while such an effect would not be present over SH land masses since Antarctica does not lie in the path of the poleward jet shift. GEOHEAT\_S and GEOHEAT have quite similar changes in the SH jet stream (Simpson et al., 2019), yet yield quite different temperature seasonal cycle changes over Antarctica, indicating that stratospheric heating is likely not the dominant mechanism of the seasonal cycle shifts in the SH high latitudes.

The results from GLENS here can also be compared with solar geoengineering simulations where solar irradiance is directly reduced without the effect of stratospheric heating. Kravitz et al. (2016) designed a solar reduction simulation (termed as the  $3 \times 3$  case) to achieve temperature goals in a similar manner as GLENS. Specifically, solar irradiance in CESM was adjusted so that the annual global mean surface temperature, interhemispheric temperature difference, and equator-to-pole temperature gradient were maintained at preindustrial levels against a 1% per year increase in atmospheric CO<sub>2</sub> (described in detailed in

section 2). To compare the GLENS and the  $3 \times 3$  case, we choose the time period of GLENS and the  $3 \times 3$  case that have the same amount of cooling relative to the high- $\text{CO}_2$  world (described in detail in section 2). It should be noted that the  $3 \times 3$  case has a preindustrial baseline that is in equilibrium, while the GLENS baseline is the RCP8.5 2010–2030 transient state. As the temperature targets are achieved, it is likely that in GLENS, this will be accompanied by relatively greater cooling of the land surface compared to the ocean than in  $3 \times 3$  (Figure S12), as the ocean will take some time to stop warming in response to the prior greenhouse gases forcing it has experienced.

The spatial pattern and magnitude of temperature seasonal anomalies in the  $3 \times 3$  case are quite similar to GLENS over the Antarctic (Figure S12 and Table S1), indicating that the seasonal variation in sunlight could be the dominant factor there. In the NH high latitudes, the spatial patterns of the shift in temperature seasonal cycle are quite different between GLENS and the  $3 \times 3$  case (Figure S12). However, a cooler summers and warmer winters are also observed in the NH high latitudes under the  $3 \times 3$  case (Figures S12 and S13), which means that the solar seasonal variation presumably also contributes to the NH changes. Under GLENS, the AOD has fairly strong seasonal variation in the NH (Figure S10), which partially compensate for the effect of seasonal variation of sunlight.

Comparisons of GLENS with related simulations (GEOHEAT, GEOHEAT\_S, and  $3 \times 3$  case) provide first-order assessments of the potential effects of stratospheric heating and the seasonal variation of sunlight in the seasonal shifts of climate change under GLENS. Under GLENS, the dynamic effect of stratospheric heating is an important contributor to the seasonal cycle shifts at high latitudes in the NH, and the seasonal variation of sunlight contributes to the seasonal cycle shifts at high latitudes in both hemispheres. An in-depth analysis of the relative importance of these two mechanisms merits further research, such as simulations with idealized aerosols that do not introduce any stratospheric heating.

## 5. Discussion and Conclusion

Solar geoengineering using stratospheric sulfate aerosols could have significant effects on the high-latitude seasonal cycle that should be taken into account in assessing the impacts of geoengineering, and hence in evaluating the benefits and risks in order to inform any future decision regarding deployment. We illustrate these effects here using the GLENS ensemble of simulations in which the aerosol injection strategy is deliberately chosen to minimize the annual mean temperature changes at high latitudes. In GLENS, the Arctic sea ice has the most pronounced seasonal cycle changes in response to undercooled winters and overcooled summers induced by sulfate aerosol geoengineering.

The effect on the seasonal cycle is less apparent in most previous studies, because typically, unless using a feedback control algorithm like in GLENS, the tropical aerosol injection leads to significant undercooling at high latitudes relative to the tropics; and thus, high-latitude impacts in prior simulations will be mostly driven by the residual changes in the annual mean. To support well-informed decisions regarding geoengineering deployment, it is reasonable to consider more complex strategies of injections, such as that used in GLENS that minimize not only the global mean temperature change but also the changes in large-scale temperature gradients.

We also analyze two other sets of relevant simulations to better understand the mechanisms of seasonal shifts under GLENS. Both seasonal variation of sunlight and aerosol-induced stratospheric heating appear to play a role in high-latitude seasonal cycle changes, but it would be premature to conclude which one is the dominant factor in the NH, especially at regional scales; the seasonal variation of sunlight appears to be dominant in the SH. More targeted simulation experiments are needed to better understand and separate the effects of the two mechanisms.

Although these mechanisms will always be present with any stratospheric sulfate aerosol geoengineering, it may be possible to devise further strategies that reduce these effects either by seasonally dependent injection strategies (Visioni et al., 2019) or through the use of alternate aerosols such as calcite that lead to less stratospheric heating (Keith et al., 2016). Our study demonstrates that the effects of the high-latitude seasonal cycle shift should be taken into account whenever we evaluate impacts from stratospheric aerosol geoengineering. The influence of high-latitude seasonal cycle change on other aspects of the Earth system, such as the carbon cycle, merits further studies.

## Acknowledgments

Jiu Jiang and Long Cao are supported by the National Key Basic Research Program of China (grant 2015CB953601), the National Natural Science Foundation of China (grants 41675063 and 41422503), and the Fundamental Research Funds for the Central Universities. Support for B. K. was provided in part by the National Science Foundation through agreement CBET-1931641, the Indiana University Environmental Resilience Institute, and the *Prepared for Environmental Change* Grand Challenge initiative. The Pacific Northwest National Laboratory is operated for the U.S. Department of Energy by Battelle Memorial Institute under contract DE-AC05-76RL01830. The CESM project is supported primarily by the National Science Foundation. Computing and data storage resources, including the Cheyenne supercomputer (doi:10.5065/D6RX99HX), were provided by the Computational and Information Systems Laboratory (CISL) at NCAR. NCAR is sponsored by the National Science Foundation. Simulation outputs are available via the Earth System Grid; see information at <https://www.cesm.ucar.edu/projects/community-projects/GLENS/>.

## References

- Barnhart, K. R., Miller, C. R., Overeem, I., & Kay, J. E. (2015). Mapping the future expansion of Arctic open water. *Nature Climate Change*, 6(3), 280–285 (2015). <https://doi.org/10.1038/nclimate2848>
- Brown, J., Ferrians, O. Jr., Heginbottom, J. A., & Melnikov, E. S. (2002). *Circum-Arctic map of permafrost and ground-ice conditions, version 2*. Colorado USA. Data available at: National Snow and Ice Data Center, Boulder. <https://nsidc.org/data/ggd318>
- Buck, H. J. (2018). Perspectives on solar geoengineering from Finnish Lapland: Local insights on the global imaginary of Arctic geoengineering. *Geoforum*, 91, 78–86. <https://doi.org/10.1016/j.geoforum.2018.02.020>
- Crutzen, P. J. (2006). Albedo enhancement by stratospheric sulfur injections: A contribution to resolve a policy dilemma? *Climatic Change*, 77(3–4), 211–220. <https://doi.org/10.1007/s10584-006-9101-y>
- DeRepentigny, P., Tremblay, L. B., Newton, R., & Pfirman, S. (2016). Patterns of sea ice retreat in the transition to a seasonally ice-free Arctic. *Journal of Climate*, 29(19), 6993–7008. <https://doi.org/10.1175/JCLI-D-15-0733.1>
- Driscoll, S., Bozzo, A., Gray, L. J., Robock, A., & Stenchikov, G. (2012). Coupled Model Intercomparison Project 5 (CMIP5) simulations of climate following volcanic eruptions. *Journal of Geophysical Research*, 117. <https://doi.org/10.1029/2012JD017607>
- Fasullo, J. T., Tilmes, S., Richter, J. H., Kravitz, B., MacMartin, D. G., Mills, M. J., & Simpson, I. R. (2018). Persistent polar ocean warming in a strategically geoengineered climate. *Nature Geoscience*, 11(12), 910–914. <https://doi.org/10.1038/s41561-018-0249-7>
- Ferraro, A. J., Charlton-Perez, A. J., & Highwood, E. J. (2015). Stratospheric dynamics and midlatitude jets under geoengineering with space mirrors and sulfate and titania aerosols. *Journal of Geophysical Research: Atmospheres*, 120, 414–429. <https://doi.org/10.1002/2014JD022734>
- Ferraro, A. J., & Griffiths, H. G. (2016). Quantifying the temperature-independent effect of stratospheric aerosol geoengineering on global-mean precipitation in a multi-model ensemble. *Environmental Research Letters*, 11, 034012. <https://doi.org/10.1088/1748-9326/11/3/034012>
- Ferraro, A. J., Highwood, E. J., & Charlton-Perez, A. J. (2014). Weakened tropical circulation and reduced precipitation in response to geoengineering. *Environmental Research Letters*, 9, 014001. <https://doi.org/10.1088/1748-9326/9/1/014001>
- Govindasamy, B., Caldeira, K., & Duffy, P. B. (2000). Geoengineering Earth's radiation balance to mitigate CO<sub>2</sub>-induced climate change. *Geophysical Research Letters*, 27, 2141–2144. <https://doi.org/10.1029/1999GL006086>
- Govindasamy, B., Caldeira, K., & Duffy, P. B. (2003). Geoengineering Earth's radiation balance to mitigate climate change from a quadrupling of CO<sub>2</sub>. *Global and Planetary Change*, 37, 157–168. [https://doi.org/10.1016/S0921-8181\(02\)00195-9](https://doi.org/10.1016/S0921-8181(02)00195-9)
- Hurrell, J. W., Holland, M. M., Gent, P. R., Ghan, S., Kay, J. E., Kushner, P. J., et al. (2013). The Community Earth System Model: A framework for collaborative research. *Bulletin of the American Meteorological Society*, 94(9), 1339–1360. <https://doi.org/10.1175/BAMS-D-12-00121.1>
- Irvine, P. J., Kravitz, B., Lawrence, M. G., & Muri, H. (2016). An overview of the Earth system science of solar geoengineering. *WIREs Climate Change*, 7(6), 815–833. <https://doi.org/10.1002/wcc.423>
- Jahn, A., Kay, J. E., Holland, M. M., & Hall, D. M. (2016). How predictable is the timing of a summer ice-free Arctic? *Geophysical Research Letters*, 43(17), 9113–9120. <https://doi.org/10.1002/2016GL070067>
- Ji, D., Fang, S., Curry, C., Kashimura, H., Watanabe, S., Cole, J., et al. (2018). Extreme temperature and precipitation response to solar dimming and stratospheric aerosol geoengineering. *Atmospheric Chemistry and Physics*, 18, 10,133–10,156. <https://doi.org/10.5194/acp-18-10133-2018>
- Kay, J. E., Deser, C., Phillips, A., Mai, A., Hannay, C., Strand, G., et al. (2014). The Community Earth System Model (CESM) large ensemble project: A community resource for studying climate change in the presence of internal climate variability. *Bulletin of the American Meteorological Society*, 96(8), 1333–1349. <https://doi.org/10.1175/BAMS-D-13-0025.1>
- Keith, D. W. (2000). Geoengineering the climate: History and prospect. *Annual Review of Energy and the Environment*, 25(1), 245–284. <https://doi.org/10.1146/annurev.energy.25.1.245>
- Keith, D. W., Weisenstein, D. K., Dykema, J. A., & Keutsch, F. N. (2016). Stratospheric solar geoengineering without ozone loss. *Proceedings of the National Academy of Sciences*, 113(52), 14,910–14,914. <https://doi.org/10.1073/pnas.1615572113>
- Kravitz, B., MacMartin, D. G., Mills, M. J., Richter, J. H., Tilmes, S., Lamarque, J.-F., et al. (2017). First simulations of designing stratospheric sulfate aerosol geoengineering to meet multiple simultaneous climate objectives. *Journal of Geophysical Research: Atmospheres*, 122, 12,616–12,634. <https://doi.org/10.1002/2017JD026874>
- Kravitz, B., MacMartin, D. G., Tilmes, S., Richter, J. H., Mills, M. J., Cheng, W., et al. (2019). Comparing surface and stratospheric impacts of geoengineering with different SO<sub>2</sub> injection strategies. *Journal of Geophysical Research: Atmospheres*, 124, 7900–7918. <https://doi.org/10.1029/2019JD030329>
- Kravitz, B., MacMartin, D. G., Wang, H., & Rasch, P. J. (2016). Geoengineering as a design problem. *Earth System Dynamics*, 7, 469–497. <https://doi.org/10.5194/esd-7-469-2016>
- Labe, Z., Magnusdottir, G., & Stern, H. (2018). Variability of Arctic sea ice thickness using PIOMAS and the CESM large ensemble. *Journal of Climate*, 31(8), 3233–3247. <https://doi.org/10.1175/JCLI-D-17-0436.1>
- Lawrence, D. M., Slater, A. G., & Swenson, S. C. (2012). Simulation of present-day and future model projection of permafrost and seasonally frozen ground conditions in CCSM4. *Journal of Climate*, 25(7), 2207–2225. <https://doi.org/10.1175/JCLI-D-11-00334.1>
- Lee, H., Ekici, A., Tjiputra, J., Muri, H., Chadburn, S., Lawrence, D. M., & Schwinger, J. (2019). The response of permafrost and high-latitude ecosystems under large scale stratospheric aerosol injection and its termination. *Earth's Future*, 7. <https://doi.org/10.1029/2018EF001146>
- Liu, X., Easter, R. C., Ghan, S. J., Zaveri, R., Rasch, P., Shi, X., et al. (2012). Toward a minimal representation of aerosols in climate models: Description and evaluation in the Community Atmosphere Model CAM5. *Geoscientific Model Development*, 5(3), 709–739. <https://doi.org/10.5194/gmd-5-709-2012>
- Meinshausen, M., Smith, S. J., Calvin, K., Daniel, J. S., Kainuma, M. L. T., Lamarque, J.-F., et al. (2011). The RCP greenhouse gas concentrations and their extensions from 1765 to 2300. *Climatic Change*, 109(1), 213. <https://doi.org/10.1007/s10584-011-0156-z>
- Mills, M. J., Richter, J. H., Tilmes, S., Kravitz, B., MacMartin, D. G., Glanville, A. A., et al. (2017). Radiative and chemical response to interactive stratospheric sulfate aerosols in fully coupled CESM1(WACCM). *Journal of Geophysical Research: Atmospheres*, 122, 13,061–13,078. <https://doi.org/10.1002/2017JD027006>
- Moore, J. C., Jevrejeva, S., & Grinsted, A. (2010). Efficacy of geoengineering to limit 21st century sea-level rise. *Proceedings of the National Academy of Sciences*, 107, 15,699–15,703. <https://doi.org/10.1073/pnas.1008153107>
- Moore, J. C., Rinke, A., Yu, X., Ji, D., & Yang, S. (2014). Arctic sea ice and atmospheric circulation under the GeoMIP G1 scenario. *Journal of Geophysical Research: Atmospheres*, 119, 567–583. <https://doi.org/10.1002/2013JD021060>

- National Research Council (2015). *Climate intervention: Reflecting sunlight to cool earth* (p. 234). Washington, DC: National Academies Press.
- Niemeier, U., & Timmreck, C. (2015). What is the limit of climate engineering by stratospheric injection of SO<sub>2</sub>? *Atmospheric Chemistry and Physics*, 15, 9129–9141. <https://doi.org/10.5194/acp-15-9129-2015>
- Oleson, K., Lawrence, D. M., Bonan, G. B., Drewniak, B., Huang, M., Koven, C. D., et al. (2013). *Technical description of version 4.5 of the Community Land Model (CLM)*. NCAR Technical Note NCAR/TN-503 + STR (p. 422). Boulder, CO: National Center for Atmospheric Research. <https://doi.org/10.5065/D6RR1W7M>
- Pitari, G., Aquila, V., Kravitz, B., Robock, A., Watanabe, S., De Luca, N., et al. (2014). Stratospheric ozone response to sulfate geoengineering: Results from the Geoengineering Model Intercomparison Project (GeoMIP). *Journal of Geophysical Research: Atmospheres*, 119, 2629–2653. <https://doi.org/10.1002/2013JD020566>
- Rasch, P. J., Crutzen, P. J., & Coleman, D. B. (2008). Exploring the geoengineering of climate using stratospheric sulfate aerosols: The role of particle size. *Geophysical Research Letters*, 35(2). <https://doi.org/10.1029/2007GL032179>
- Rasch, P. J., Tilmes, S., Turco, R. P., Robock, A., Oman, L., Chen, C.-C., et al. (2008). An overview of geoengineering of climate using stratospheric sulphate aerosols. *Philosophical Transactions of the Royal Society A: Mathematical, Physical and Engineering Sciences*, 366 (1882), 4007–4037. <https://doi.org/10.1098/rsta.2008.0131>
- Richter, J. H., Tilmes, S., Mills, M. J., Tribbia, J., Kravitz, B., MacMartin, D. G., et al. (2017). Stratospheric dynamical response and ozone feedbacks in the presence of SO<sub>2</sub> injections. *Journal of Geophysical Research: Atmospheres*, 122, 12,557–12,573. <https://doi.org/10.1002/2017JD026912>
- Robock, A., & Mao, J. (1992). Winter warming from large volcanic eruptions. *Geophysical Research Letters*, 19, 2405–2408. <https://doi.org/10.1029/92GL02627>
- Robock, A., Oman, L., & Stenchikov, G. L. (2008). Regional climate responses to geoengineering with tropical and Arctic SO<sub>2</sub> injections. *Journal of Geophysical Research*, 113. <https://doi.org/10.1029/2008JD010050>
- Rogelj, J., den Elzen, M., Höhne, N., Fransen, T., Fekete, H., Winkler, H., et al. (2016). Paris Agreement climate proposals need a boost to keep warming well below 2°C. *Nature*, 534(7609), 631–639. <https://doi.org/10.1038/nature18307>
- Shindell, D. T., Schmidt, G. A., Mann, M. E., & Faluvegi, G. (2004). Dynamical winter climate response to large tropical volcanic eruptions since 1600. *Journal of Geophysical Research*, 109, D05104. <https://doi.org/10.1029/2003JD004151>
- Simpson, I. R., Tilmes, S., Richter, J. H., Kravitz, B., MacMartin, D. G., Mills, M. J., et al. (2019). The regional hydroclimate response to stratospheric sulfate geoengineering and the role of stratospheric heating. *Journal of Geophysical Research: Atmospheres*, 124. <https://doi.org/10.1029/2019JD031093>
- Slater, A. G., & Lawrence, D. M. (2013). Diagnosing present and future permafrost from climate models. *Journal of Climate*, 26(15), 5608–5623. <https://doi.org/10.1175/jcli-d-12-00341.1>
- Stenchikov, G. L., Kirchner, I., Robock, A., Graf, H. -F., Antuña, J. C., Grainger, R. G., et al. (1998). Radiative forcing from the 1991 Mount Pinatubo volcanic eruption. *Journal of Geophysical Research: Atmospheres*, 103(D12), 13,837–13,857. <https://doi.org/10.1029/98JD00693>
- Thompson, D. W. J., & Wallace, J. M. (2001). Regional climate impacts of the Northern Hemisphere annular mode. *Science*, 293(5527), 85–89. <https://doi.org/10.1126/science.1058958>
- Tilmes, S., Müller, R., & Salawitch, R. (2008). The sensitivity of polar ozone depletion to proposed geoengineering schemes. *Science*, 320(5880), 1201–1204. <https://doi.org/10.1126/science.1153966>
- Tilmes, S., Richter, J. H., Kravitz, B., MacMartin, D. G., Mills, M. J., Simpson, I. R., et al. (2018). CESM1(WACCM) Stratospheric aerosol geoengineering large ensemble project. *Bulletin of the American Meteorological Society*, 99(11), 2361–2371. <https://doi.org/10.1175/bams-d-17-0267.1>
- van den Broeke, M., Bamber, J., Ettema, J., Rignot, E., Schrama, E., van de Berg, W. J., et al. (2009). Partitioning recent Greenland mass loss. *Science*, 326(5955), 984–986. <https://doi.org/10.1126/science.1178176>
- van Vuuren, D. P., Edmonds, J., Kainuma, M., Riahi, K., Thomson, A., Hibbard, K., et al. (2011). The representative concentration pathways: An overview. *Climatic Change*, 109(1), 5. <https://doi.org/10.1007/s10584-011-0148-z>
- Visioni, D., MacMartin, D. G., Kravitz, B., Tilmes, S., Mills, M. J., Richter, J. H., & Boudreau, M. P. (2019). Seasonal injection strategies for stratospheric aerosol geoengineering. *Geophysical Research Letters*, 46, 7790–7799. <https://doi.org/10.1029/2019GL083680>
- Visioni, D., Pitari, G., Aquila, V., Tilmes, S., Cionni, I., De Genova, G., & Mancini, E. (2017). Sulfate geoengineering impact on methane transport and lifetime: Results from the Geoengineering Model Intercomparison Project (GeoMIP). *Atmospheric Chemistry and Physics*. <https://doi.org/10.5194/acp-17-11209-2017>
- Wei, L., Ji, D., Miao, C., Muri, H., & Moore, J. C. (2018). Global streamflow and flood response to stratospheric aerosol geoengineering. *Atmospheric Chemistry and Physics*, 18, 16,033–16,050. <https://doi.org/10.5194/acp-18-16033-2018>
- Wunderlich, F., & Mitchell, D. M. (2017). Revisiting the observed surface climate response to large volcanic eruptions. *Atmospheric Chemistry and Physics*, 17, 485–499. <https://doi.org/10.5194/acp-17-485-2017>